International Journal of Nanomedicine

Dovepress
open access to scientific and medical research

Open Access Full Text Article

ORIGINAL RESEARCH

Biomineralization-Inspired Anti-Caries Strategy Based on Multifunctional Nanogels as Mineral Feedstock Carriers

Rui Yuan[1,*], Yuwen Zhang[1,*], Liqiong Liao[2], Yige Ge[1], Weichang Li[1], Qinghui Zhi[1]

[1]Hospital of Stomatology, Guanghua School of Stomatology, Guangdong Provincial Key Laboratory of Stomatology, Sun Yat-sen University, Guangzhou, Guangdong, 510030, People's Republic of China; [2]Biomaterials Research Center, School of Biomedical Engineering, Southern Medical University, Guangzhou, Guangdong, 510515, People's Republic of China

*These authors contributed equally to this work

Correspondence: Qinghui Zhi, Hospital of Stomatology, Guanghua School of Stomatology, Guangdong Provincial Key Laboratory of Stomatology, Sun Yat-Sen University, Guangzhou, Guangdong, 510055, People's Republic of China, Email zhiqingh@mail.sysu.edu.cn; Weichang Li, Hospital of Stomatology, Guangdong Provincial Key Laboratory of Stomatology, Sun Yat-Sen University, Guangzhou, Guangdong, 510055, People's Republic of China, Email liwch57@mail.sysu.edu.cn

International Journal of Nanomedicine downloaded from https://www.dovepress.com/
For personal use only.

Background: Dentin caries remains a significant public concern, with no clinically viable material that effectively combines remineralization and antimicrobial properties. To address this issue, this study focused on the development of a bio-inspired multifunctional nanogel with both antibacterial and biomineralization properties.

Methods: First, p(NIPAm-co-DMC) (PNPDC) copolymers were synthesized from N-isopropylacrylamide (NIPAm) and 2-methacryloyloxyethyl-trimethyl ammonium chloride (DMC). Subsequently, PNPDC was combined with γ-polyglutamic acid (γ-PGA) through physical cross-linking to form nanogels. These nanogels served as templates for the mineralization of calcium phosphate (Cap), resulting in Cap-loaded PNPDC/PGA nanogels. The nanogels were characterized using various techniques, including TEM, particle tracking analysis, XRD, and FTIR. The release properties of ions were also assessed. In addition, the antibacterial properties of the Cap-loaded PNPDC/PGA nanogels were evaluated using the broth microdilution method and a biofilm formation assay. The remineralization effects were examined on both demineralized dentin and type I collagen in vitro.

Results: PNPDC/PGA nanogels were successfully synthesized and loaded with Cap. The diameter of the Cap-loaded PNPDC/PGA nanogels was measured as 196.5 nm at 25°C and 162.3 nm at 37°C. These Cap-loaded nanogels released Ca^{2+} and PO_4^{3-} ions quickly, effectively blocking dental tubules with a depth of 10 μm and promoting the remineralization of demineralized dentin within 7 days. Additionally, they facilitated the heavy intrafibrillar mineralization of type I collagen within 3 days. Moreover, the Cap-loaded nanogels exhibited MIC_{50} and MIC_{90} values of 12.5 and 50 mg/mL against *Streptococcus mutans*, respectively, with an MBC value of 100 mg/mL. At a concentration of 50 mg/mL, the Cap-loaded nanogels also demonstrated potent inhibitory effects on biofilm formation by *Streptococcus mutans* while maintaining good biocompatibility.

Conclusion: Cap-loaded PNPDC/PGA nanogels are a multifunctional biomimetic system with antibacterial and dentin remineralization effects. This strategy of using antibacterial nanogels as mineral feedstock carriers offered fresh insight into the clinical management of caries.

Keywords: nanomaterial, mineralization, antibacterial materials, dentinal tubule occlusion, caries

Introduction

Dental caries remains a public health concern that can cause oral pain and gingival abscesses, food intolerance, nutritional deficiencies, malocclusions, and other conditions that severely reduce quality of life.[1] Caries in children younger than six is called early childhood caries (ECC) and remains a serious problem in both developed and developing countries due to its high prevalence and low treatment rates.[2] Caries, including ECC, occurs when cariogenic microorganisms, primarily *Streptococcus mutans (S. mutans)*, decompose carbohydrates to produce acids, leading to the

Received: 11 May 2023
Accepted: 28 August 2023
Published: 4 September 2023

© 2023 Yuan et al. This work is published and licensed by Dove Medical Press Limited. The full terms of this license are available at https://www.dovepress.com/terms.php and incorporate the Creative Commons Attribution – Non Commercial (unported, v3.0) License (http://creativecommons.org/licenses/by-nc/3.0/). By accessing the work you hereby accept the Terms. Non-commercial uses of the work are permitted without any further permission from Dove Medical Press Limited, provided the work is properly attributed. For permission for commercial use of this work, please see paragraphs 4.2 and 5 of our Terms (https://www.dovepress.com/terms.php).

Graphical Abstract

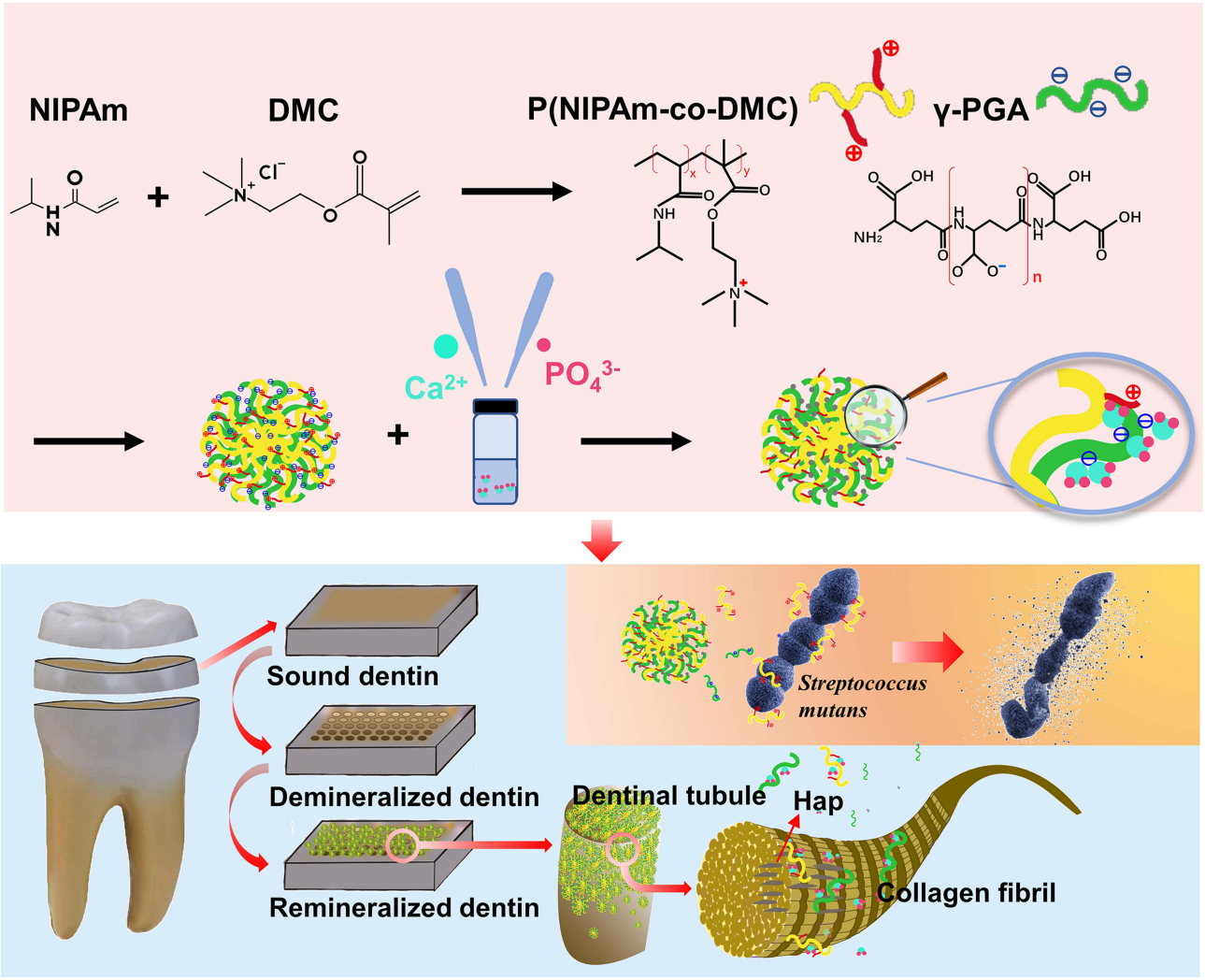

demineralization of dental inorganic materials and the decomposition of collagen organic matter and thus to the progressive formation of cavities.[3] Currently, the treatment of dental caries is still based on traditional resin fillings and remineralization drugs. However, many children are too young to tolerate prolonged filling treatments and require general anaesthesia, which is expensive and increases the risks of treatment.[4] The remineralization drugs currently used for ECC treatments are mainly fluorides, and silver diamine fluoride (SDF) is the most widely used. However, SDF tastes bitter and causes discoloration of dentin,[5] and its potential toxicity has long been a concern.[6,7] In addition, SDF cannot produce mineral feedstocks such as calcium ions (Ca^{2+}) and phosphate (PO_4^{3-}), and the structure of remineralized tissue formed after the treatment is far from that of dentin. Therefore, identifying an ideal material that provides stable mineral ion sources and can safely control cariogenic microorganisms is highly desirable.

Numerous studies have demonstrated that biomineralization strategies are a promising approach in caries management.[8,9] Biomineralization is a typically dynamic bioprocess by which organisms generate mineralized tissues, including bone and teeth, in a hierarchical fashion. Dentin is a collagenous structure consisting mainly of type I collagen, which is mineralized intrafibrillarly and extrafibrillarly with carbonated hydroxyapatite (HAp), and the intrafibrillar mineralization determines the mechanical properties of dentin.[10] Another important component of dentin, noncollagenous

proteins (NCPs), plays a key role in regulating dentin remineralization. Numerous materials inspired by NCPs have been developed for the remineralization of teeth, among which polymer-induced liquid precursor (PILP) is the most popular. In the PILP approach, charged polymers mimic the functions of NCPs, stabilize amorphous calcium phosphate (ACP), and then mediate the transformation of ACP into HAp crystals inside collagen fibres.[11] Although this strategy has achieved gratifying success in promoting dentin mineralization, the mineral precursor fluid system must be prepared fresh to ensure stability and effectiveness, which limits its clinical transformation. Additionally, during the PILP process, it is necessary to constantly replenish the polymers, Ca^{2+} and PO_4^{3-} to enable mineralization, and it is difficult to keep the mineralizing solution in the demineralization area until the mineralization process is finished.[12] In addition, with repeated demineralization events due to persistent acid production by cariogenic bacteria, the efficiency of remineralization will be greatly reduced.[13] In addition, antibacterial activities play a key role in dental remineralization. In summary, the development of a stable remineralization system that provides mineral resources while exerting antimicrobial effects remains a challenge.

Biomineralization itself provides important clues for the design of new remineralization biomaterials. Nanogels, which are hydrogel particles composed of cross-linked polymers, exhibit adjustable chemical and physical properties, good mechanical properties, and high biocompatibility.[14] In this study, we developed a type of polymer-based nanogel as the mineralization template, loaded calcium phosphate (Cap) into the nanogel first to form a stable nanocomplex, and then allowed the nanogels to carry the remineralization feedstock into dentin tubules (DTs). Based on this clue, NIPAm (N-isopropylacrylamide) and 2-methacryloyloxyethyltrimethylammonium chloride (DMC), a quaternary ammonium salt (QAS), were used to synthesize the copolymer p(NIPAm-co-DMC) (PNPDC). QAS is one of the most widely used antimicrobials,[15–17] and NIPAm is a typical monomer used to prepare temperature-sensitive hydrogels that can achieve controlled drug release at human body temperature.[18–20] Then, the anionic polymer γ-polyglutamic acid (γ-PGA) was added to form nanogels by physical cross-linking, and Cap was loaded. The carboxyl groups enriched in γ-PGA can act as nucleation sites for Cap, which is the key to the use of nanogels as mineralized templates.[21] The hypotheses to be tested were as follows: 1) Cap could be loaded into PNPDC/PGA nanogels and release enough ions for remineralization, and the ion release process could be regulated by temperature; 2) Cap-loaded PNPDC/PGA nanogels could induce both intra- and extrafibrillar mineralization; and 3) Cap-loaded PNPDC/PGA nanogels exert antibacterial effects against *S. mutans* with good biocompatibility.

Materials and Methods

Materials

N-isopropylacrylamide (NIPAm, 97%, M.W. 113.16 g/mol) was purchased from Sigma–Aldrich, and 2-methacryloyloxyethyl-trimethyl ammonium chloride (DMC), 4-(2-hydroxyethyl)-1-piperazineethanesulfonic acid (HEPES), azoisobutyronitrile (AIBN), tetrahydrofuran (THF), dipotassium phosphate (K_2HPO_4), calcium chloride dihydrate ($CaCl_2{\cdot}2H_2O$), sodium hydroxide (NaOH), sodium chloride (NaCl), ethanol and ammonia were all obtained from Shanghai Macklin Biochemical Technology Co., Ltd. Poly-γ-glutamic acid (γ-PGA, Mw=2000 kDa) was purchased from Yuanye Biotechnology Co., Ltd. (Shanghai, China). All chemicals were used as received without further purification.

Preparation of p(NIPAm-Co-DMC) (PNPDC)

The typical polymer synthesis procedure was performed as follows. One hundred millilitres of THF was placed in a 250 mL round-bottom flask. Next, DMC (0.3 mol) and NIPAm (0.1 mol) monomers and AIBN initiator (1 mmol) were slowly added to THF. The molar ratio of DMC and NIPAm monomers was always three to one. Afterwards, the round bottom flask was heated in a water bath at 60–65°C, and the reaction mixtures were stirred at 600 rpm/min for 18 h under a nitrogen atmosphere. The polymerization reaction was stopped by cooling the mixture to room temperature. The crude product was then obtained by rotary steaming. The excess unreacted monomer and initiator were removed by multiple ultrafiltration steps using deionized water at room temperature for at least 3 days, changing the water every eight hours. After several purification columns and freeze-drying, the PNPDC copolymer was obtained.

Preparation of PNPDC/PGA Nanogels

For the synthesis of PNPDC/PGA nanogels, a PNPDC homogeneous solution (5 mg/mL) was added to the PGA solution (5 mg/mL) dropwise under stirring, and the reaction was carried out for 24 h at room temperature at 600 rpm/min. After the reaction was completed, the precipitates were separated by centrifugation at 10,000 rpm/min, washed alternately with water and ethanol, and collected by freeze-drying.

Calcium Phosphate (Cap) Loading

The PNPDC/PGA nanogels were first dissolved in HEPES buffer (pH=7.4) to form a homogeneous solution (10 mg/mL). The nanogel suspension was then poured into a $CaCl_2$ solution (pH=7.4, 18 mmol/L) of the same volume and stirred for 2 h at room temperature to form a stable complex of nanogels and Ca^{2+}. Subsequently, a K_2HPO_4 aqueous solution (pH=7.4, 4.2 mmol/L) was dripped into the Ca-nanogel solution. The reaction was carried out for 24 h at room temperature. After the reaction was completed, the precipitates were separated through centrifugation at 10,000 rpm/min, washed alternately with water and ethanol, and then collected by freeze-drying. In this reaction, the $CaCl_2$ solution and K_2HPO_4 aqueous solution were prepared with HEPES buffer to maintain a pH of 7.4.

Nanogel Characterization

The sizes and morphologies of the Cap-loaded PNPDC/PGA nanogels were observed via transmission electron microscopy (FEI Tecnai G2 Spirit, Netherlands). The nanogels were dispersed in ddH_2O, treated with ultrasound and dropped onto a 300-mesh copper mesh (Beijing Zhongjingkeyi Technology Co., Ltd). During this process, the acceleration voltage was maintained at 120 kV. A particle tracking analyser (Particle Metrix, Germany) was also utilized to examine the zeta potentials and size distributions of the nanogels. Fifty milligrams of the nanogels was blended with 5 mL of water with sonication to form a homogeneous suspension and diluted two hundred times before the test. X-ray diffraction (Rigaku D/Max-IIIA/PC, Japan) was employed to analyse the phase composition of the nanogels under 40 kV per 100 mA and 3500 CPS for the Cu target. Fourier transform infrared (FTIR) spectra were acquired by using a PerkinElmer 2000 spectrometer (NICOLET 6700, Thermo, USA) with KBr pellets at wavelengths ranging from 4000 to 400 cm^{-1}, a resolution of 1 cm^{-1} and an average of 64 scans. The release of Ca^{2+} was detected following the protocol of a calcium assay kit (Arsenazo III method). Nanogels were dispersed in TBS buffer (10 mg/mL) without Ca^{2+} or PO_4^{3-}, and the Ca^{2+} concentration was measured after 12 h, 1 d, 2 d, 3 d, 5 d, and 7 d at 25°C and 37°C. The release of PO_4^{3-} was detected following the protocol of a phosphate assay kit (phosphomolybdic acid method), and the concentration was also measured after 12 h, 1 d, 2 d, 3 d, 5 d, and 7 d at 25°C and 37°C.

Antibacterial Test Against *Streptococcus Mutans*

Determination of MIC (Minimum Inhibitory Concentration) and MBC (Minimum Bactericidal Concentration)

To explore the bacteriostatic effect of Cap-loaded PNPDC/PGA nanogels, an in vitro bacteriostasis experiment against *S. mutans* UA159 was performed using the broth microdilution method.[22] Microbes were grown overnight in brain heart infusion (BHI, Difco, USA) broth at 37°C with 5% CO_2 and then adjusted to a final concentration of 2×10^6 CFU in BHI broth. The Cap-loaded PNPDC/PGA nanogels serially diluted to the desired concentrations from 5 mg/mL to 400 mg/mL (gradient dilution) were added to each well, followed by equal amounts of bacterial suspension (100 μL). The mixtures were then incubated for 24 h, and a microplate reader was used to evaluate cell growth at 600 nm absorbance (OD 600). Then, 200 μL of cultured bacteria was removed from each well, spread on BHI solid medium and cultured for 48 h for colony counting. The MIC was determined as the minimum nanogel concentration that completely inhibited the visible growth of *S. mutans* by measuring the OD value at 600 nm using an enzyme marker. The MBC was defined as the lowest concentration at which no colony formed on the plates.

Biofilm Formation Assay

The formation of *S. mutans* biofilms was evaluated through a crystal violet assay, a live/dead fluorescence staining assay and scanning electron microscope (SEM) observation. Briefly, the Cap-loaded nanogel suspension was serially diluted with BHIs (BHI medium containing 1% sucrose) in 96-well plates (0–100 mg/mL, 100 μL/well),[23] and *S. mutans* grown

overnight and diluted to 10^6 CFU/mL was added to each well (100 μL/well). Blank control samples consisted of BHIs without nanogels or bacteria, and negative control samples consisted of BHIs with bacteria. After incubation for 24 h at 37°C with 5% CO_2, the medium was decanted, and each well was washed twice with PBS to remove nonadherent bacteria. Anhydrous methanol was used to fix the adhered biofilms at the bottom of the wells. Afterwards, the biofilms were stained using 0.1% crystal violet for 15 min. The wells were washed with running water to remove the unbound dye and air dried to release the bound dye. Then, 200 μL of 95% ethanol was added to each well and shaken for 30 min. Finally, the absorbance at 600 nm was recorded to estimate the biofilm volume. The minimum biofilm inhibitory concentration (MBIC) was defined as the lowest concentration of antimicrobial agent necessary to inhibit biofilm formation.

Confocal laser scanning microscopy (CLSM) (Olympus, Olympus FV3000, Japan) was used to observe the distribution of live/dead bacteria and the 3D structure of biofilms. *S. mutans* biofilms were incubated on confocal dishes with or without the addition of nanogels at concentrations of 25–200 mg/mL and rinsed with PBS to remove floating bacteria. The biofilms were then stained with 2.5 μM SYTO 9 and propidium iodide (Invitrogen, USA) as described previously[24] and observed by CLSM with a 40× lens objective (Olympus FV3000, Japan), and the percentages of live and dead cells were quantified using COMSTAT image-processing software.

For SEM observation, biofilms were formed following the methods used in CLSM assays and crystal violet assays and cultured on sterile coverslips with strong adhesion. Then, the biofilms were fixed with 2.5% glutaraldehyde for 4 h, dehydrated with graded ethanol (30% to 100%), treated with tert-butanol and freeze-dried. The samples were sputtered with gold before being observed with a scanning electron microscope (SEM) system (Hitachi S-4800, Japan).

Assessment of Tubule-Occluding Effects and Dentin Remineralization

Sound maxillary third molars were obtained from donors (18 to 25 years of age) with informed consent under a protocol approved by the Medical Ethics Committee of Hospital of Stomatology Sun Yat-sen University review board (KQEC-2022-86-01). An exposed dentin surface was obtained by using a wheel cutter (WEIYEE, China) under stable water irrigation perpendicular to the long axis of the tooth. The section was then cut into a 4 mm×4 mm×2 mm dentin block. The dentin surface far from the pulp was retained as the experimental surface, and the remaining surfaces were sealed with acid-resistant nail polish. The experimental surfaces were polished with SiC abrasive papers from 400 to 5000 grit, and then the dentin blocks were ultrasonically cleaned for 10 min. The blocks were prescreened with AFM to exclude those with occluded tubules. The certified specimens were dipped into 1% citric acid (pH 3.8) for 2 min to ensure patency of the dentinal tubules and ultrasonically washed for 10 min before application. A Cap-loaded PNPDC/PGA nanogel suspension (10 mg/mL, TBS) was applied at 37°C for 7 days, and TBS buffer (pH = 7.4) was applied to disks by the same method as a control. Afterwards, the mineralization of dentin was scanned using SEM (Hitachi S-4800, Japan).

Hardness is an important indicator to assess the effect of dentin remineralization. Microhardness measurements were performed using a microhardness tester (HMV-2T SHIMADZU, Tokyo, Japan). Indentations were made within 15s from the loading (0.01 kg) for all specimens, and the values were automatically transformed into the Vickers hardness number by the tester.

Mineralization of Type I Collagen Fibrils

A single-layer collagen fibril model was used to examine the mineralization ability of the nanogels. The model was reconstituted according to the literature.[25] Rat tail tendon fascicles from mature SD rats (60 days old) were retrieved in iso-osmotic saline. Ten milligrams of rat tail tendon collagen was dissolved in 100 mL of 0.1 M acetic acid (pH 3.0) overnight. Collagen stock solution (0.1 mg/mL) was neutralized in an ammonia gas atmosphere for 4 h, and single layers of type I collagen were reconstructed on nickel TEM grids. The neutralized collagen solution was incubated at 37°C for 3 days to allow gelation. Cross-linking was induced in the reconstituted collagen fibrils by floating the collagen-coated grids upside-down in 0.3 M EDC/0.06 M NHS solution for 4 h. Thereafter, the collagen-coated grids were rinsed with Milli-Q water and air-dried. The collagen-coated grids were mineralized by floating the grids upside-down over the Cap-loaded nanogel suspension (10 mg/mL, TBS) for 24 h or 72 h at 37°C. Afterwards, the mineralization of type I collagen was scanned using a transmission electron microscope (FEI Tecnai G2 Spirit, Netherlands) without further staining.

Evaluation of Biocompatibility

Cell viability was determined using a cell counting kit-8 (CCK-8; Dojindo Laboratories, Japan).[26] In brief, human gingival epithelial cells (hGECs) cultured in medium (10% foetal bovine serum, 90% α-MEM and 1% penicillin/streptomycin) were incubated in a 96-well microplate for 24 h (3000 cells per well). Then, solutions of nanogels at different concentrations (0–100 mg/mL) were added for further incubation for 1 day, 3 days, and 5 days. After each time point, the CCK-8 working solution (10 μL/well) was added to each well and incubated at 37°C for 2 h. The OD of the solution in each well was measured at 450 nm. The cell viability of different groups was calculated according to the kit instructions. Each concentration was independently assayed three times with three technical replicates. Based on ISO 10993–5, cell viability above 80% was considered to indicate that the concentration was noncytotoxic; 80–60% indicated weak cytotoxicity; 60–40% indicated moderate cytotoxicity; and below 40% indicated strong cytotoxicity.[27]

The proliferative activities and morphologies of cells were visually observed by staining under the same experimental conditions. After the cells were further incubated with different concentrations of nanogels for 1 day, 3 days, and 5 days, the culture medium was removed, and medium containing calcein-AM (2 μM) and propidium iodide (4 μM) was used to stain the live and dead cells, respectively. Afterwards, the cells were gently washed with PBS. The cells were imaged using CLSM with a 10× lens objective (Olympus FV3000, Japan).[28]

Statistical Analysis

All statistical analyses were performed with OriginPro 2022 SR1 and SAS version 9.4, and the data are presented as the means ± standard deviations (SDs). For multiple group comparisons, P values were derived from one-way ANOVA (continuous variables) or chi-square analysis (categorical variables). A p value <0.05 was considered to indicate statistical significance for all comparisons.

Results and Discussion

Characterization of the Nanogels

The typical morphology of the nanogels with cross-linked structures is shown in Figure 1a–d. Before the loading of Cap (Figure 1a and b), PNPDC and γ-PGA formed spherical nanogels with diameter of 79.08±5.27 nm. After Cap loading, nanogels with a smaller diameter (72.52±2.49 nm) were formed, and uniformly distributed high-density crystallization points appeared inside (Figure 1c and d). The results obtained from selected area electron diffraction (SAED) show the formation of crystals. The X-ray diffraction (XRD) patterns of the nanogels also showed that before loading with Cap, no diffraction peaks were observed, but peaks at 27.4°, 28.5°, 31.8°, 45.4°, and 56.5° were observed for the Cap-loaded PNPDC/PGA nanogels (Figure 1e). These peaks closely coincided with those for Hap.[29] Fourier transform infrared (FTIR) spectra of the Cap PNPDC/PGA nanogels and Cap-free PNPDC/PGA nanogels are shown in Figure 1f. The peak at 1467 cm^{-1} was attributed to the methylene groups linked to N^+ in the quaternary ammonium group of PNPDC. The characteristic peak of PNIPAm were located at 3147 cm^{-1} (secondary amide N-H stretching), and the peaks at 1710 cm^{-1} were attributed to the carbonyl groups of PGA.[30] Additionally, PO_4 bands were observed at 1103 cm^{-1}, suggesting that Cap was present in the Cap PNPDC/PGA nanogels.[31] These results demonstrated that the PNPDC/PGA nanogels were successfully synthesized and that Cap was loaded into the nanogels. Notably, the intrinsic cross-linked structure of the nanogels was not destroyed by the addition of Cap.

The use of a self-assembled polymer scaffold as a template for crystallization has been reported in a previous study, and the matrix was employed as a template for calcium carbonate, where amorphous calcium carbonate was imbibed into the internal structure.[32] In this study, using a self-assembled polymer, nanogel, as a mineralization template, small CaP nuclei were generated alongside the γ-PGA chain, clustered into small spheres, and converted into low-crystallinity hydroxyapatite (HAp). In light of crystallization theory,[33] the nanogels created a very small space for crystal nucleation, and the ion consumption associated with crystal nucleus formation led to a continuous depletion of supersaturation and thus the driving force for critical nucleus formation. However, this could limit the size of the Cap nuclei formed, even preventing nucleation from solution supersaturations that would yield bulk crystals. Thus, Cap can be loaded into self-assembled nanogels with suitable crystallinity and release ions in a suitable environment, which will facilitate the

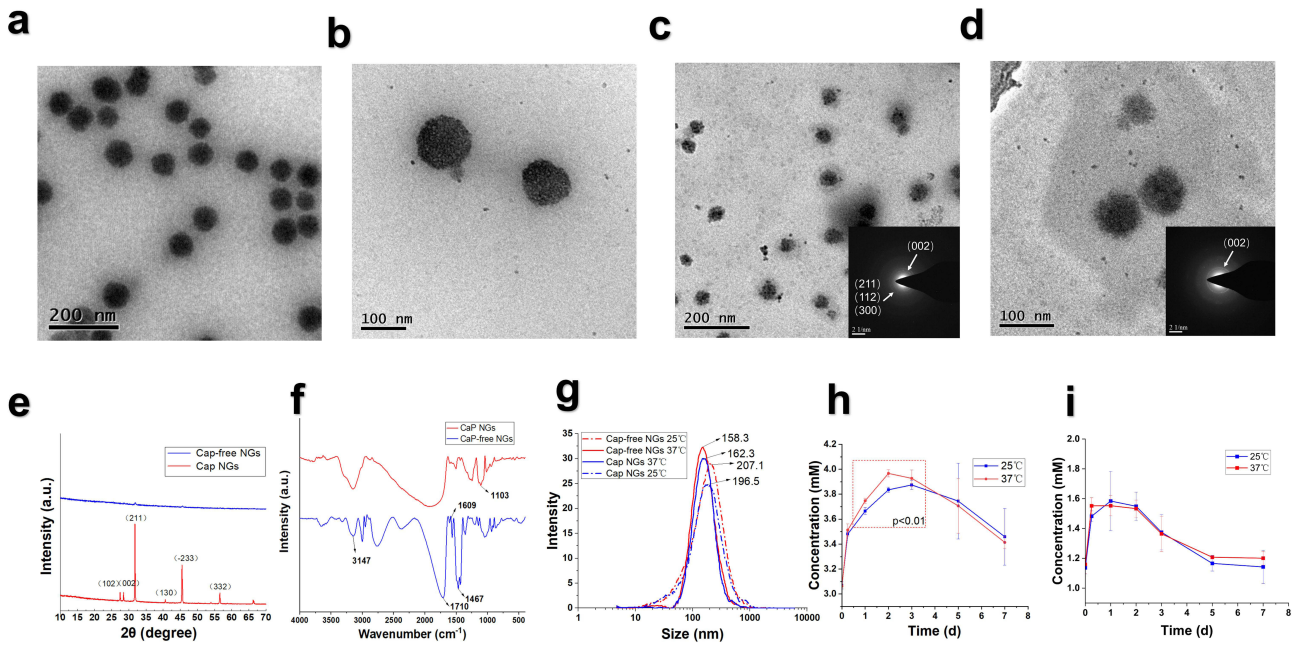

Figure 1 Characterization of PNPDC/PGA nanogels with or without Cap loading. (**a** and **b**) TEM observation of the PNPDC/PGA nanogels, which are round particles with a uniform network structure inside. (**c** and **d**) TEM observation of the Cap-loaded PNPDC/PGA nanogels and the results of selected area electron diffraction (SAED) show crystal formation inside the nanogels. (**e** and **f**) XRD and FTIR spectra results of the PNPDC/PGA nanogels with or without Cap loading. (**g**) Nanoparticle size tracker results of the nanogels at 37°C and 25°C. (**h**) In vitro Ca^{2+} release of the Cap-loaded PNPDC/PGA nanogels at 37°C and 25°C. (**i**) In vitro PO_4^{3-} release of the Cap-loaded PNPDC/PGA nanogels at 37°C and 25°C.

Abbreviations: Cap-free NGs, PNPDC/PGA nanogels without loaded Cap; Cap NGs, Cap-loaded PNPDC/PGA nanogels.

transport of Cap by the nanogels to the demineralized areas of the dentin and release ions to promote remineralization. Otherwise, overly stable and highly crystalline HAp will be detrimental to the release of ions and to the achievement of intrafibrillar mineralization.

In addition, the temperature responsiveness of the nanogels was explored. The size range of nanogels at different temperatures was analysed by performing nanoparticle tracking analysis using a ZetaView particle tracker from ParticleMetrix (Figure 1g). The mean particle size of PNPDC/PGA nanogels was 207.1 nm at 25°C and 158.3 nm at 37°C, and the mean particle size of Cap-loaded PNPDC/PGA nanogels was 196.5 nm at 25°C and 162.3 nm at 37°C. Notably, the volume observed is smaller than that in aqueous solution due to the swelling property and because the nanogels are dry under TEM observation. As dentinal tubules have diameters exceeding 2 μm, the nanogels could easily reach deep into the DTs due to their size advantages. In addition, the volume of the nanogels shrinks when the temperature rises to 37°C, facilitating their entry into the DTs. The effect of temperature on nanogels was also demonstrated in in vitro ion release experiments. As shown in Figure 1h, within three days of incubation at 37°C or 25°C in TBS buffer, the amount of Ca^{2+} increased rapidly. During the initial stage, Ca^{2+} was released in burst mode at 0–2 days and then slowly from 2 to 3 days at both 37°C and 25°C. As the temperature affected the Ca^{2+} release, the concentration of Ca^{2+} in the solution at 37°C was always higher than that at 25°C from 0 to 2 days, with a statistically significant difference (p=0.003). On the third day, however, the release of Ca^{2+} reached saturation, and Cap began to deposit; therefore, so the free Ca^{2+} in the aqueous solution began to decrease sharply. The change in PO_4^{3-} concentration exhibited a similar trend to the release of Ca^{2+}. PO_4^{3-} was released in burst mode at 0–1 day and then slowly from 1 to 2 days, but there was no significant difference at different temperatures (Figure 1i). This might be because the measured PO_4^{3-} concentration was too low to show the variation. The release of ions was accompanied by the dissociation of Cap PNPDC/PGA nanogels. The TEM results showed the shape of the nanogels at different times, and obvious mineral deposition could be observed at 3 days at 37°C and 25°C (Figure S1). These results suggest that the nanogels easily decomposed and released ions simultaneously, promoting remineralization. On the other hand, the release rate of Ca^{2+} at 37°C was faster than that at 25°C, which may occur for two reasons. One is that the temperature increase accelerated the

degradation of nanogels, and the other is that the temperature responsiveness of PNIPAm promoted drug release. At temperatures below the LCST, hydrogen bonds form between the hydrophilic groups on NIPAm and water molecules. However, the hydrogen bonds between the polymer and water break at higher temperatures, causing the hydrophobic group on NIPAm to become dominant. As a result, the polymer chain shrinks, causing the nanogel volume to shrink.[34] The nanogels exhibited a degree of temperature-controlled Ca^{2+} release.

Although PNIPAm hydrogels have previously been mixed with HAp for DT occlusion, this mixed form is not conducive to ion release and remineralization.[35] The purpose of loading calcium phosphate into nanogels was to release Ca^{2+} and PO_4^{3-}, the primary minerals involved in mineralizing dentin, into the DTs for remineralization.[36] In the in vitro ion release experiments (Figure 1h and i), the Ca^{2+} release amount reached 4.0 mM at a low concentration of the nanogels (10 mg/mL), and the PO_4^{3-} release amount reached 1.6 mM. These ion concentrations are very similar to those in conventional remineralizing solutions and are effective for remineralization.[9] To our knowledge, this is the first time that nanogels have been used as carriers of Cap for remineralization therapy.

Cap-Loaded PNPDC/PGA Nanogels Exhibited Resistance to Bacterial Multiplication and Biofilm Formation

S. mutans is the main pathogen that causes dental caries to occur and develop,[3] and it is crucial for anti-caries materials to exhibit antibacterial activity against *S. mutans*. However, antibacterial properties are rarely considered in traditional biomineralization materials. Traditional antibacterial drugs are prone to resistance, and the formation of plaque biofilm also hinders the action of antibacterial drugs.[37] To solve this problem, in this study, we synthesized copolymer chains rich in quaternary ammonium salt (QAS) groups to prepare nanogels with antibacterial activity. The antibacterial activity of the nanogels was evaluated by a plate microdilution assay, and an in vitro model of *S. mutans* biofilms was established to evaluate the effects of the nanogels on the biofilm formation of cariogenic bacterial species. When tested by the plate microdilution method, the nanogel MIC_{50} and MIC_{90} values were 12.5 and 50 mg/mL, respectively, and the MBC value was 100 mg/mL, at which point no colonies formed on the plates (Figure 2a and d). The antibacterial performance of the nanogels was concentration dependent, and the higher the concentration was, the better the antibacterial effect.

Bacterial biofilms are the main causes of infectious diseases,[38] and dental plaque formed by *S. mutans* is another fundamental factor leading to the occurrence and development of dental caries.[3] Therefore, materials that can inhibit the formation of plaque biofilm or remove existing biofilm are important for preventing and treating dental caries. The results of this study showed that the Cap-loaded PNPDC/PGA nanogels significantly inhibited the formation of *S. mutans* biofilms at concentrations not lower than the MIC_{90} (Figure 2). According to the results of the crystal violet experiment, when the concentration of nanogels reached 50 mg/mL, the amount of biofilm formed decreased sharply, and almost no biofilm was observed (Figure 2f and g). The live/dead fluorescent assay showed similar results to those of the crystal violet assay (Figure 2c and e). With increasing nanogel concentration, the amount of biofilm formed was significantly reduced, and the dead/live ratio was increased considerably. The SEM results (Figures 2b and S2) showed that the bacteria in contact with the material (50 mg/mL) swelled, deformed, and lysed into fragments. It is now believed that the antibacterial function of QAS was mainly derived from the high cation concentration they carried, which provided these compounds with high surface activity. Because of this activity, the cations were adsorbed on the cell surfaces, and hydrophobic chains penetrated the membrane, which destroyed the membrane and caused the leakage of intracellular substances, such as potassium ions or DNA.[39]

To modify oral materials for antibacterial activity, various metal ions are widely used, among which silver ions are the most commonly studied.[40] Although silver ions show good antibacterial activity, the cytotoxicity of metal ions should not be ignored.[41,42] QASs are more biocompatible.[43] When developing oral materials, antibacterial activity and biocompatibility should be fully considered and balanced. Although the nanogels used in this study are electronegative due to the addition of PGA, the gels easily decompose into PNPDC and PGA chains, and PNPDC has a strong positive charge, which may be the main reason the nanogels exhibited antibacterial activity. Therefore, the excellent antibacterial properties of the nanogels used in this study provide a promising solution to the continuous challenge caused by bacteria while treating caries.

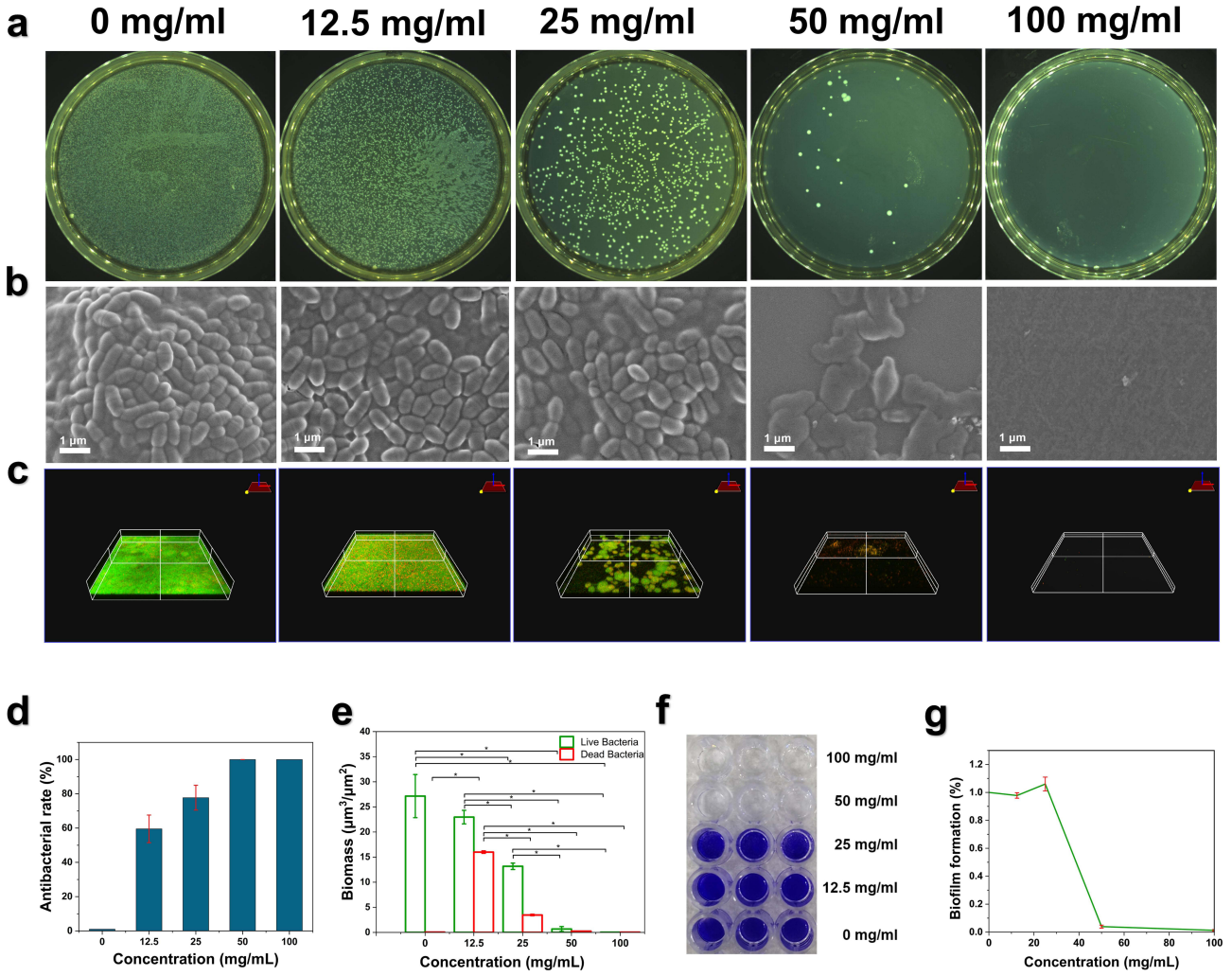

Figure 2 Assessment of the antibacterial activity of the Cap-loaded PNPDC/PGA nanogels. (**a**) The growth inhibition rate (%) of *S. mutans* cells after treatment with nanogels was determined using plate count method. The nanogels were tested at concentrations ranging from 0 to 100 mg/mL for a duration of 24 hours. (**b**) SEM observation of *S. mutans* UA159 biofilm under the action of different concentrations of the nanogels. (**c**) CLSM and stereo 3D rendering images of the preformed biofilm of *S. mutans* UA159 treated with different concentrations of the nanogels. Live cells stained with SYTO 9 (green) and dead cells stained with PI (red). (**d**) Antibacterial rate calculated from plate count results. (**e**) Live and dead bacteria biomass calculated from live/dead bacteria staining results. (**f** and **g**) Crystal violet assay and visualized by OD 600 nm. *p<0.01.

Cap-Loaded PNPDC/PGA Nanogels Accelerated Dentin Remineralization and DTs Occlusion

To evaluate the potential application of Cap-loaded PNPDC/PGA nanogels for the treatment of caries, their effect on dentin remineralization was investigated using an in vitro model. Before acid etching, the dentin tubules were completely embolized by minerals (Figure S3), and after acid etching, the dentin showed empty dentinal tubules (Figure 3a–c). Due to the small size of the PNPDC/PGA nanogels (approximately 200 nm in the solution state), they should easily enter the deep DTs (approximately 2 μm in diameter), where remineralization is expected. After the Cap-loaded nanogels were applied on the surface of demineralized dentine for 7 days, the peony-patterned material was connected into networks and sheets and completely blocked the dentine tubules (Figures 3g–i and S4). On these surfaces, based on energy dispersive spectroscopy analysis, phosphorus (P), calcium (Ca) and oxygen (O) were the main components of the elemental composition, and the Ca/P ratio of the newly deposited minerals reached a value of 1.8 (Figure 3j), which was similar to that of HAp. From the transverse section perpendicular to the DTs, the depth of materials and minerals occluding the DTs exceeded 10 μm (Figure 3g), with similar or even better effects than those in a previous study.[44–46] At the same time, the DTs were still empty and remineralization did not happen after treated with TBS buffer in the control

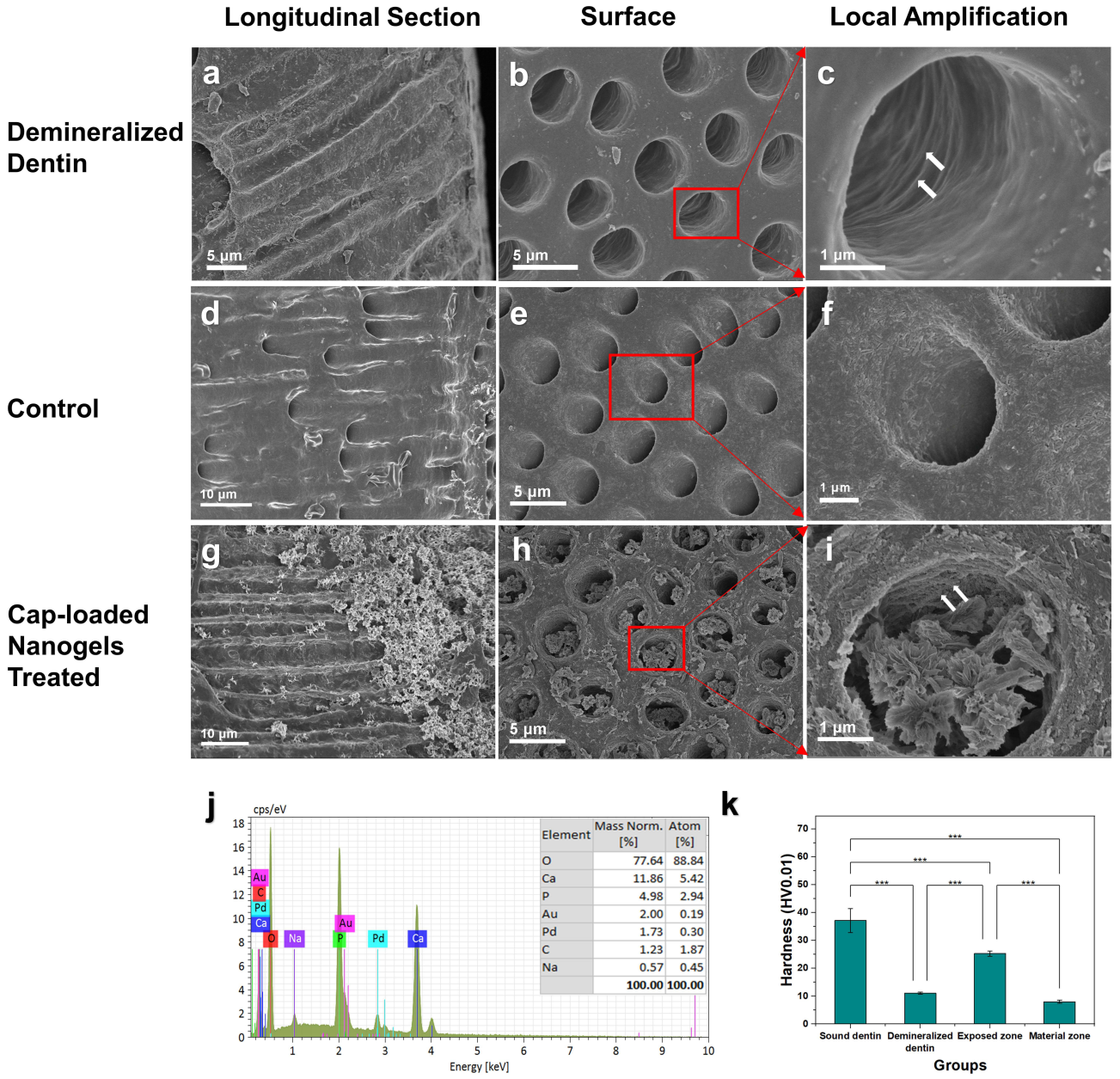

Figure 3 Cap-loaded PNPDC/PGA nanogels accelerated dentin remineralization and DTs occlusion. (**a–c**) SEM micrographs of demineralized dentin observed from the longitudinal section (**a**) and surface (**b–c**). c: A higher magnification view of the boxed area showing demineralized collagens can be observed (arrows). (**d–i**) SEM micrographs of dentin surface treated without (**d–f**) or with the Cap-loaded nanogels (**g–i**) for 7 days, and views from the longitudinal section (**d** and **g**) and the surface (**e** and **f**), (**h** and **i**) can be observed. (**i**) Magnified view of tubule showing precipitate crystal and nanogel growth in dentin tubules and remineralized collagens can be observed (arrows). (**j**) Spectra from energy-dispersive analysis show the elemental composition of phosphorus (P), Calcium (Ca), and oxygen (O), which were the main components of the Cap-loaded nanogel-treated dentin surface. (**k**) Microhardness of the dentin surface with or without Cap-loaded nanogel treatment. After remineralization, the exposed zone without nanogel coating and the coated zone had totally different hardness values due to the nanogel characteristics. ***$p<0.001$.

group (Figure 3d–f). These results suggested that the deposited minerals and nanogels showed an excellent occlusion effect.

Microhardness was also calculated. The sound dentin specimens showed optimal mechanical performance with a value of 37.2 ± 4.3 HV0.01 (Figure 3k). However, the hardness of the dentin was significantly weakened to 11.08 ± 0.34 HV0.01 after acid etching. On the other hand, the mechanical strength of demineralized dentine was significantly improved by nanogel treatment, with a value of 25.28±0.97 HV0.01 on the exposed uncoated area, although the mechanical strength was still lower than that of natural dentin. However, the nanogel-coated zone showed lower hardness

than the demineralized dentin because the nanogel treatment significantly promoted the remineralization of demineralized dentin and partially restored its hardness, but the nanogels themselves were relatively soft due to their inherent properties.

Cap-Loaded PNPDC/PGA Nanogels Accelerated Intrafibrillar Remineralization on Type I Collagen Models

The type I collagen scaffold is the most abundant organic substance in dentin and constitutes the greatest difference between enamel and dentin. Intrafibrillar mineralization significantly enhances the mechanical strength of dentin by creating an organic–inorganic hybrid.[47] In this study, the capacity of the Cap-loaded PNPDC/PGA nanogels to mediate the intrafibrillar mineralization of collagen fibrils was evaluated. As Figure 4 shows, unstained collagen that was mineralized for 24 h (Figure 4a and b) and 72 h (Figure 4c and d) formed intrafibrillar apatite crystallization. Acicular and fusiform intrafibrillar crystallites were observed inside the mineralized fibril and alongside the longitudinal axis of the collagen fibril (write arrows). In addition, partially and heavily mineralized collagen both became more straight and rigid, instead of exhibiting the limp and bent shape of pure collagen (Figure S5). These results indicate that ordered mineralization of collagen fibres, producing a structure similar to that of naturally mineralized collagen, can be achieved with the Cap-loaded PNPDC/PGA nanogels.

Biologically, the formation of crystalline apatite is initiated by performing heterogeneous nucleation of inorganic calcium phosphate on an organic extracellular matrix.[48] The results confirmed that the Cap-loaded PNPDC/PGA nanogels released Ca/P, which suggested that dentin remineralization is possible. In the oral environment, the Cap PNPDC/PGA nanogels underwent degradation and disintegrated into active Cap debris relatively quickly, therefore providing continual Ca^{2+} release and inducing calcium overload. After acting on the demineralized dentin surface, the nanogels entered the DTs with a penetration depth greater than 10 μm and released Cap to realize remineralization; in

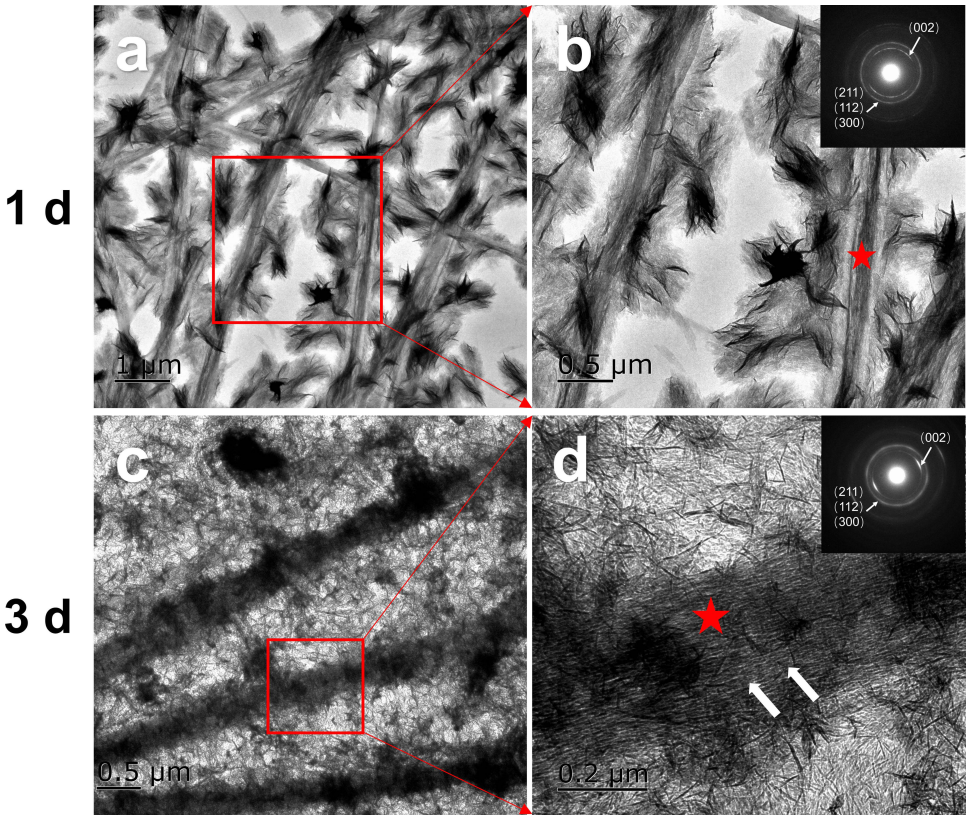

Figure 4 Cap-loaded PNPDC/PGA nanogel-mediated intrafibrillar mineralization of reconstructed collagen fibrils. Unstained TEM images of collagen fibrils mineralized with the nanogels for 1 day (**a** and **b**) and 3 days (**c** and **d**). After mineralization of collagen for 1 d, needle-shaped intrafibrillar crystallites could be seen within the partially mineralized fibril. Similar to the image in 3 d, high magnification of a heavily mineralized collagen fibril showing electron-dense mineral strands within the fibril (arrows). Selected area electron diffraction (SAED) shows apatite crystallites aligned along the fibril's c-axis (red asterisk).

addition, heavy intrafibrillar remineralization was observed on the collagen treated with nanogels for 3 days. Since researchers first achieved intrafibrillar mineralization in vitro, the mechanism has remained controversial. Although a series of theories have been proposed in the past few decades, the importance of polymers in achieving intrafibrillar remineralization remains unquestionable. PILP is among the most popular concepts.[10] In the PILP process, the charged polymer sequesters ions and generates liquid–liquid-phase separation within the crystallizing solution, forming nanoscopic droplets with a highly hydrated ACP phase. This PILP procedure begins with the formation of an amorphous liquid-phase mineral precursor, which enables intrafibrillar mineralization. This is because the fluidic characteristics of the amorphous precursor phase allow the precursor to enter the interior space of collagen fibrils by capillary action. Upon loss of hydration water, the precursor solidifies and crystallizes into a more thermodynamically stable phase, leaving the collagen fibrils embedded with nanoscopic HAp crystals.[11] In this study, first, the nanogels released sufficient Ca^{2+} and PO_4^{3-} to achieve remineralization, which could be demonstrated in the ion release assays. Second, the degraded components of the nanogels could play the role of noncollagenous proteins (NCPs) to stabilize the calcium phosphate precursor to form PILP. Previous studies have demonstrated that both cationic and anionic polymers can stabilize calcium and phosphorus ions to form PILP.[25] Cap-loaded PNPDC/PGA nanogels could be resolved into PNPDC and γ-PGA, which are both charged polymers that may stabilize ACP. This might be the theoretical basis of how the nanogels achieve intrafibrillar remineralization.

Another important theory regarding intrafibrillar remineralization is the Gibbs-Donnan equilibrium theory, which was proposed by Niu et al.[25] In addition to the electrostatic gravity theory proposed in previous studies, this theory further highlights the polymer-induced changes in the internal and external osmotic pressure of collagen fibres and their contribution to the driving force of intrafibrillar remineralization. Simply, the presence of polymer outside the fibre increases the osmotic pressure outside the fibre, causing the collagen fibre to shrink, transporting the ACP into the fibre during collagen fibre volume recovery, and finally causing the mineralized crystals to deposit in the collagen fibre. Based on this theory, in this study, the nanogels and the polymers produced from these gels increased the osmotic pressure outside the collagen fibres, and γ-PGA also strongly adsorbed water, which is conducive to the formation of intrafibrillar remineralization.

Biocompatibility

In recent years, researchers have focused much attention on the safety of nanomaterials. Some materials applied to the tooth surface may dissolve into the saliva, enter the gastrointestinal tract, or even be absorbed into the blood.[49] Therefore, biosafety is an important factor that must be considered when developing materials to treat caries. The calcein-AM/PI staining assay and CCK-8 assay showed that at 100 mg/mL, the Cap PNPDC/PGA nanogels significantly decreased hGEC proliferation, while the Cap PNPDC/PGA nanogels showed no significant influence on hGEC proliferation at 50 mg/mL and below (Figure 5).

The biocompatibility of nanomaterials is greatly influenced by the synthesis process. Nanogels can be divided into those obtained by chemical cross-linking and those obtained by physical cross-linking. During chemical cross-linking process, cross-linking agents, initiators, surfactants and other toxic substances must be introduced, which limits the clinical transformation of nanogels to a certain extent. However, physical cross-linking uses the hydrogen bonds formed between polymer macromolecules, van der Waals forces, hydrophobic forces, electrostatic interactions, etc., so introducing toxic cross-linkers, catalysts, or by-products as small-molecule cytotoxic substances is not necessary.[50] Previous studies have fully confirmed the strong biocompatibility of pNIPAm and QAS-pNIPAm.[51,52] γ-PGA, a common food and skin care additive, also exhibits excellent biocompatibility and degradability.[53,54] Another possible source for cytotoxicity of the nanogels is the release of CaP; however, in previous studies, Ca-induced cytotoxicity was specifically selective in tumour cells but biologically safe in normal cells. Tumour cells utilize different calcium metabolism and homeostasis processes from normal cells.[55,56] In this study, when the concentration was 50 mg/mL, the nanogels were noncytotoxic. The MIC_{90} and the MBIC of the nanogels were both 50 mg/mL, which was a suitable concentration to achieve antibacterial functions. Compared to multifunctional anti-caries materials in previous studies,[44,57,58] the nanogels were easier to store, which was beneficial for clinical translation. The achievement of intrafibrillar mineralization also made the material more suitable for dentin remineralization in addition to enamel remineralization. It should be noted that from

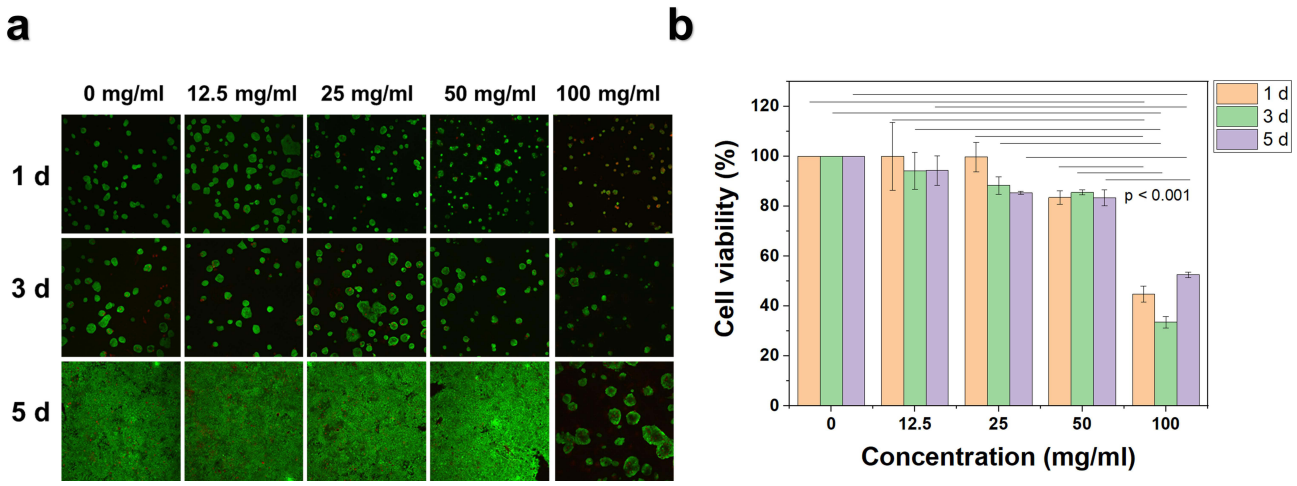

Figure 5 Biocompatibility of the Cap-loaded PNPDC/PGA nanogels. (**a**) Calcein-AM/PI staining assay of human gingival epithelial cells cultured with different concentrations of nanogels for 1, 3, and 5 days. Calcein-AM was used to stain live cells, and propidium iodide (PI) was used to stain dead cells. (**b**) Cell viability of human gingival epithelial cells cultured with different concentrations of the nanogels for 1, 3, and 5 days. Relative viability was determined by CCK-8 assay.

current findings and results, the suitable concentration used for remineralization was 10 mg/mL, so If we desire a material with dual functions at the same concentration, we need to find a compromise concentration. That is, alternative concentrations of Cap-loaded nanogels may also exhibit these dual functionalities, albeit suboptimal for each individual function. This is a major limitation of the present study, and we need to do further experiments to determine optimal concentrations for different scenarios.

Conclusion

In this study, a systematic synthesis approach was established to prepare Cap-loaded PNPDC/PGA nanogels based on the concept of biomineralization. The physically cross-linked PNPDC/PGA nanogels were synthesized first to serve as the mineralization template, and Cap was loaded as low-crystallinity HAp. Cap, as well as charged polymers resulting from the decomposition of nanogels, could be used as feedstocks for mineralization based on the PILP concept. The Cap-loaded PNPDC/PGA nanogels could induce intrafibrillar and interfibrillar remineralization in the dentin and collagen model as well as occlude DTs, inhibit the growth and biofilm formation of *S. mutans*, and show good biocompatibility. This strategy of using nanogels to deliver mineral feedstock to the interior of demineralized dentin is effective and shows good prospects for clinical caries management.

Acknowledgments

This work was supported by the National Natural Science Foundation of China [grant number 21905094].

Disclosure

The authors report no conflicts of interest in this work.

References

1. Mathur VP, Dhillon JK. Dental caries: a disease which needs attention. *Indian J Pediatr*. 2018;85(3):202–206. doi:10.1007/s12098-017-2381-6
2. Tinanoff N, Baez RJ, Diaz Guillory C, et al. Early childhood caries epidemiology, aetiology, risk assessment, societal burden, management, education, and policy: global perspective. *Int J Paediatr Dent*. 2019;29(3):238–248. doi:10.1111/ipd.12484
3. Selwitz RH, Ismail AI, Pitts NB. Dental Caries. *Lancet*. 2007;369(9555):51–59. doi:10.1016/S0140-6736(07)60031-2
4. Sinner B, Becke K, Engelhard K. General anaesthetics and the developing brain: an overview. *Anaesthesia*. 2014;69(9):1009–1022. doi:10.1111/anae.12637
5. Duangthip D, Jiang M, Chu CH, et al. Non-surgical treatment of dentin caries in preschool children--systematic review. *BMC Oral Health*. 2015;15:44. doi:10.1186/s12903-015-0033-7
6. Fancher ME, Fournier S, Townsend J, et al. Cytotoxic effects of silver diamine fluoride. *Am J Dent*. 2019;32(3):152–156.

7. Hu S, Muniraj G, Mishra A, et al. Characterization of silver diamine fluoride cytotoxicity using microfluidic tooth-on-a-chip and gingival equivalents. *Dent Mater*. 2022;38(8):1385–1394. doi:10.1016/j.dental.2022.06.025
8. Pandya M, Diekwisch TGH. Enamel biomimetics-fiction or future of dentistry. *Int J Oral Sci*. 2019;11(1):8. doi:10.1038/s41368-018-0038-6
9. Cao CY, Mei ML, Li QL, et al. Methods for biomimetic remineralization of human dentine: a systematic review. *Int J Mol Sci*. 2015;16 (3):4615–4627. doi:10.3390/ijms16034615
10. Oosterlaken BM, Vena MP, de With G. In Vitro Mineralization of Collagen. *Adv Mater*. 2021;33(16):e2004418. doi:10.1002/adma.202004418
11. Olszta MJ, Cheng X, Jee SS, et al. Bone structure and formation: a new perspective. *Mater Sci Eng*. 2017;58(3–5):77–116.
12. Chen Z, Duan Y, Shan S, et al. Deep and compact dentinal tubule occlusion via biomimetic mineralization and mineral overgrowth. *Nanoscale*. 2022;14(3):642–652. doi:10.1039/D1NR05479A
13. Lemos JA, Palmer SR, Zeng L, et al. The Biology of *Streptococcus mutans*. *Microbiol Spectr*. 2019;7(1):10.1128/microbiolspec.GPP3-0051–2018.
14. Ahmed S, Alhareth K, Mignet N. Advancement in nanogel formulations provides controlled drug release. *Int J Pharm*. 2020;584:119435. doi:10.1016/j.ijpharm.2020.119435
15. Yang Y, Shi K, Yu K, et al. Degradable hydrogel adhesives with enhanced tissue adhesion, superior self-healing, cytocompatibility, and antibacterial property. *Adv Healthcare Mater*. 2022;11(4):e2101504. doi:10.1002/adhm.202101504
16. Rukmanikrishnan B, Jo C, Choi S, et al. Flexible ternary combination of gellan gum, sodium carboxymethyl cellulose, and silicon dioxide nanocomposites fabricated by quaternary ammonium silane: rheological, thermal, and antimicrobial properties. *ACS Omega*. 2020;5 (44):28767–28775. doi:10.1021/acsomega.0c04087
17. Gonzalez-Henriquez CM, Sarabia-Vallejos MA, Rodriguez-Hernandez J. Advances in the fabrication of antimicrobial hydrogels for biomedical applications. *Materials*. 2017;10(3):232. doi:10.3390/ma10030232
18. Ferguson CTJ, Huber N, Landfester K, et al. Dual-responsive photocatalytic polymer nanogels. *Angew Chem Int Ed Engl*. 2019;58 (31):10567–10571. doi:10.1002/anie.201903309
19. Pilipenko I, Korzhikov-Vlakh V, Valtari A, et al. Mucoadhesive properties of nanogels based on stimuli-sensitive glycosaminoglycan-graft-pNIPAAm copolymers. *Int J Biol Macromol*. 2021;186:864–872. doi:10.1016/j.ijbiomac.2021.07.070
20. Rey M, Fernandez-Rodriguez MA, Karg M, et al. Poly- N -isopropylacrylamide nanogels and microgels at fluid interfaces. *Acc Chem Res*. 2020;53 (2):414–424. doi:10.1021/acs.accounts.9b00528
21. Xiaoyu M, Xiuling D, Chunyu Z, et al. Polyglutamic acid-coordinated assembly of hydroxyapatite nanoparticles for synergistic tumor-specific therapy. *Nanoscale*. 2019;11(32):15312–15325. doi:10.1039/C9NR03176F
22. Serna N, Sanchez-Garcia L, Sanchez-Chardi A, et al. Protein-only, antimicrobial peptide-containing recombinant nanoparticles with inherent built-in antibacterial activity. *Acta Biomater*. 2017;60:256–263. doi:10.1016/j.actbio.2017.07.027
23. Zaidi S, Singh SL, Khan AU. Exploring antibiofilm potential of bacitracin against *streptococcus mutans*. *Microb Pathog*. 2020;149:104279. doi:10.1016/j.micpath.2020.104279
24. Bijle MN, Ashraf U, Abdalla MM, et al. Biofilm modulatory response of arginine-fluoride varnish on multi-species biofilm. *J Dent*. 2022;122:104096. doi:10.1016/j.jdent.2022.104096
25. Niu LN, Jee SE, Jiao K, et al. Collagen intrafibrillar mineralization as a result of the balance between osmotic equilibrium and electroneutrality. *Nat Mater*. 2017;16(3):370–378. doi:10.1038/nmat4789
26. Zhang QJ, Liu Y, Zhang WT, et al. Synthesis, antifungal activity, and cytotoxicity of AgBr-NP@CTMAB hybrid and its application in PMMA. *Int J Nanomedicine*. 2021;16:3091–3103. doi:10.2147/IJN.S290673
27. Standard I. *Biological Evaluation of Medical Devices. Part 5: Tests for in vitro Cytotoxicity*. Geneva, Switzerland: International Organization for Standardization; 2009.
28. Ge Y, Wang C, Zhang W, et al. Coassembly behavior and rheological properties of a β-hairpin peptide with dicarboxylates. *Langmuir*. 2021;37 (40):11657–11664. doi:10.1021/acs.langmuir.1c01376
29. Kawata M, Azuma K, Izawa H, et al. Biomineralization of calcium phosphate crystals on chitin nanofiber hydrogel for bone regeneration material. *Carbohydr Polym*. 2016;136:964–969. doi:10.1016/j.carbpol.2015.10.009
30. Elashnikov R, Slepicka P, Rimpelova S, et al. Temperature-responsive PLLA/PNIPAM nanofibers for switchable release. *Mater Sci Eng*. 2017;72:293–300. doi:10.1016/j.msec.2016.11.028
31. Izawa H, Nishino S, Maeda H, et al. Mineralization of hydroxyapatite upon a unique xanthan gum hydrogel by an alternate soaking process. *Carbohydr Polym*. 2014;102:846–851. doi:10.1016/j.carbpol.2013.10.080
32. Finnemore AS, Scherer MR, Langford R, et al. Nanostructured calcite single crystals with gyroid morphologies. *Adv Mater*. 2009;21(38–39):3928–3932. doi:10.1002/adma.200900615
33. Meldrum FC, O'Shaughnessy C. Crystallization in Confinement. *Adv Mater*. 2020;32(31):e2001068. doi:10.1002/adma.202001068
34. Wu DQ, Zhu J, Han H, et al. Synthesis and characterization of arginine-NIPAAm hybrid hydrogel as wound dressing: in vitro and in vivo study. *Acta Biomater*. 2018;65:305–316. doi:10.1016/j.actbio.2017.08.048
35. Tempesti P, Nicotera GS, Bonini M, et al. Poly(N-isopropylacrylamide)-hydroxyapatite nanocomposites as thermoresponsive filling materials on dentinal surface and tubules. *J Colloid Interface Sci*. 2018;509:123–131. doi:10.1016/j.jcis.2017.09.001
36. Liang K, Wang S, Tao S, et al. Dental remineralization via poly(amido amine) and restorative materials containing calcium phosphate nanoparticles. *Int J Oral Sci*. 2019;11. doi:10.1038/s41368-019-0048-z
37. Brown ED, Wright GD. Antibacterial drug discovery in the resistance era. *Nature*. 2016;529(7586):336–343. doi:10.1038/nature17042
38. Yan J, Bassler BL. Surviving as a community: antibiotic tolerance and persistence in bacterial biofilms. *Cell Host Microbe*. 2019;26(1):15–21. doi:10.1016/j.chom.2019.06.002
39. Tischer M, Pradel G, Ohlsen K, et al. Quaternary ammonium salts and their antimicrobial potential: targets or nonspecific interactions? *ChemMedChem*. 2012;7(1):22–31. doi:10.1002/cmdc.201100404
40. Chen H, Gu L, Liao B, Zhou X, Cheng L, Ren B. Advances of Anti-Caries Nanomaterials. *Molecules*. 2020;25(21):5047. doi:10.3390/molecules25215047
41. Wu J, Wang L, He J, et al. In vitro cytotoxicity of Cu^{2+}, Zn^{2+}, Ag^{+} and their mixtures on primary human endometrial epithelial cells. *Contraception*. 2012;85(5):509–518. doi:10.1016/j.contraception.2011.09.016

42. Akter M, Sikder MT, Rahman MM, et al. A systematic review on silver nanoparticles-induced cytotoxicity: physicochemical properties and perspectives. *J Adv Res*. 2018;9:1–16. doi:10.1016/j.jare.2017.10.008
43. Padnya PL, Terenteva OS, Akhmedov AA, et al. Thiacalixarene based quaternary ammonium salts as promising antibacterial agents. *Bioorg Med Chem*. 2021;29:115905. doi:10.1016/j.bmc.2020.115905
44. He J, Yang J, Li M, et al. Polyzwitterion manipulates remineralization and antibiofilm functions against dental demineralization. *ACS Nano*. 2022;16(2):3119–3134. doi:10.1021/acsnano.1c10812
45. Song J, Wang H, Yang Y, et al. Nanogels of carboxymethyl chitosan and lysozyme encapsulated amorphous calcium phosphate to occlude dentinal tubules. *J Mater Sci Mater Med*. 2018;29(6):84. doi:10.1007/s10856-018-6094-9
46. Jung J-H, Park S-B, Yoo K-H, et al. Effect of different sizes of bioactive glass-coated mesoporous silica nanoparticles on dentinal tubule occlusion and mineralization. *Clin Oral Investig*. 2019;23(5):2129–2141. doi:10.1007/s00784-018-2658-9
47. Balooch M, Habelitz S, Kinney JH, et al. Mechanical properties of mineralized collagen fibrils as influenced by demineralization. *J Struct Biol*. 2008;162(3):404–410. doi:10.1016/j.jsb.2008.02.010
48. He H, Shao C, Mu Z, et al. Promotion effect of immobilized chondroitin sulfate on intrafibrillar mineralization of collagen. *Carbohydr Polym*. 2020;229:115547. doi:10.1016/j.carbpol.2019.115547
49. Zor F, Selek FN, Orlando G, et al. Biocompatibility in regenerative nanomedicine. *Nanomedicin*. 2019;14(20):2763–2775. doi:10.2217/nnm-2019-0140
50. Sasaki Y, Akiyoshi K. Nanogel engineering for new nanobiomaterials: from chaperoning engineering to biomedical applications. *Chem Rec*. 2010;10(6):366–376.
51. Shen J, Chen R, Wang J, et al. One-step surface modification strategy with composition-tunable microgels: from bactericidal surface to cell-friendly surface. *Colloids Surf B Biointerfaces*. 2022;212:112372. doi:10.1016/j.colsurfb.2022.112372
52. Qi M, Song Z, Wang L, et al. Effect of temperature-sensitive nanogel combined with angioplasty on sICAM-1 and VE-cadherin in lower extremity arterial occlusion rabbits. *Bioengineered*. 2021;12(2):12535–12543. doi:10.1080/21655979.2021.2009967
53. Hu ZZ, Sha XM, Ye YH, et al. Effects of gamma-polyglutamic acid on the gelling properties and non-covalent interactions of fish gelatin. *J Texture Stud*. 2020;51(3):511–520. doi:10.1111/jtxs.12495
54. Manocha B, Margaritis A. Production and characterization of gamma-polyglutamic acid nanoparticles for controlled anticancer drug release. *Crit Rev Biotechnol*. 2008;28(2):83–99. doi:10.1080/07388550802107483
55. Pesakhov S, Nachliely M, Barvish Z, et al. Cancer-selective cytotoxic Ca^{2+} overload in acute myeloid leukemia cells and attenuation of disease progression in mice by synergistically acting polyphenols curcumin and carnosic acid. *Oncotarget*. 2016;7(22):31847–31861. doi:10.18632/oncotarget.7240
56. Moghtaderi H, Sepehri H, Attari F. Combination of arabinogalactan and curcumin induces apoptosis in breast cancer cells in vitro and inhibits tumor growth via overexpression of P53 level in vivo. *Bio Pharmacot*. 2017;88:582–594. doi:10.1016/j.biopha.2017.01.072
57. Toledano M, Muñoz-Soto E, Aguilera FS, et al. The mineralizing effect of zinc oxide-modified hydroxyapatite-based sealer on radicular dentin. *Clin Oral Investig*. 2020;24(1):285–299. doi:10.1007/s00784-019-02938-5
58. Xu X, Wang N, Wu M, et al. Programmed antibacterial and mineralization therapy for dental caries based on zinc-substituted hydroxyapatite/alendronate-grafted polyacrylic acid hybrid material. *Colloids Surf B Biointerfaces*. 2020;194:111206. doi:10.1016/j.colsurfb.2020.111206

International Journal of Nanomedicine Dovepress

Publish your work in this journal

The International Journal of Nanomedicine is an international, peer-reviewed journal focusing on the application of nanotechnology in diagnostics, therapeutics, and drug delivery systems throughout the biomedical field. This journal is indexed on PubMed Central, MedLine, CAS, SciSearch®, Current Contents®/Clinical Medicine, Journal Citation Reports/Science Edition, EMBase, Scopus and the Elsevier Bibliographic databases. The manuscript management system is completely online and includes a very quick and fair peer-review system, which is all easy to use. Visit http://www.dovepress.com/testimonials.php to read real quotes from published authors.

Submit your manuscript here: https://www.dovepress.com/international-journal-of-nanomedicine-journal